SEMARAK ILMU PUBLISHING

CFD Letters

Journal homepage:
https://semarakilmu.com.my/journals/index.php/CFD_Letters/index
ISSN: 2180-1363

URANS Prediction of the Hydrodynamic Interactions of Two Ship-like Floating Structures in Regular Waves

Fahmy Ardhiansyah[1], Rudi Walujo Prastianto[1,*], Eko Budi Djatmiko[1], Ketut Suastika[2]

[1] Department of Ocean Engineering, Faculty of Marine Technology, Institut Teknologi Sepuluh Nopember (ITS), 60111 Surabaya, Indonesia
[2] Department of Naval Architecture, Faculty of Marine Technology, Institut Teknologi Sepuluh Nopember (ITS), 60111 Surabaya, Indonesia

ARTICLE INFO

Article history:
Received 20 November 2023
Received in revised form 21 December 2023
Accepted 23 January 2024
Available online 31 July 2024

Keywords:
URANS CFD; gap influence; hydrodynamic interaction; ship-like floating structure; side-by-side configuration

ABSTRACT

A side-by-side configuration of floating structures is commonly used in ocean exploration practices, such as offshore vessels for loading and offloading, floating cranes, and offshore floating wind turbines. Computational Fluid Dynamics (CFD) method is current practice for the analysis of hydrodynamic interactions of the side-by-side vessels. The purpose of this study is yo carry out a benchmark study of CFD method applied for the above analysis. URANS CFD method was applied utilizing a k-ε turbulence model and a volume of fluid (VOF) method to capture the free surface. Different ratios of wave length to vessel's length and different gaps between between the vessels were considered in the study. Simulation results show that the wave length to vessel's length ratio λ/L affects significantly the wave pattern around the vessels and inside the gap. For the shorter waves, the gap influences the wave pattern both inside and outside the gap. Further, the pressure distribution on the keel surface of the vessels is asymmetric about the vertical center plane along the vessel, which resulted in roll motion eventhough the vessel is in head seas. Roll motion was observed in all gap variations considered. Amplitude modulation was observed in the heave and pitch motions, while generation of side-band frequency components were observed in the roll motion, which indicate a non-linear fluid-structure interaction.

1. Introduction

A side-by-side configuration of floating structures is commonly used in ocean exploration practices. This configuration is widely employed in the oil and gas industries for loading and offloading operations between two vessels arranged in close pair formation [1, 2]. In addition, a side-by-side configuration is frequently applied as floating crane vessels to lift and install structural modules on floating or fixed platforms [3, 4]. The renewable energy industry also uses side-by-side configuration in the installation of offshore floating wind turbines [5]. In all the above applications, special attention is required on the complex hydrodynamic interactions between the two-adjacent floating structures.

* *Corresponding author.*
E-mail address: rudiwp@oe.its.ac.id (Rudi Walujo Prastianto)

https://doi.org/10.37934/cfdl.16.12.117

Floating body interaction studies were primarily performed through model tests in the 1960s to 1990s, and later developed into numerical potential flow models in the early 2000s. Newton [6] discussed the hydrodynamic interactions of side-by-side floating vessels in deep water, in which he considered the interaction of two-adjacent ships in an experimental study. Experimental results showed a coupled force and moment effect due to the two interacting ships. Subsequently, Remery [7] reported an experimental study to investigate moored ship mooring forces due to passing ships in shallow water. The study was carried out in a wave basin using a 1:100 model scale to represent a fully loaded 100,000 deadweight tonnage (DWT) tanker. The interaction between moored ships and passing ships is crucial for the prediction of the lateral mooring forces. In addition to experimental studies, Newman [8] conducted a numerical study on multi-body interaction, in which he introduced a free surface patch to capture the hydrodynamic interaction effects.

The fast advancement in computer and computational techniques in the last few decades has made computational fluid dynamics (CFD) currently a standard approach for solving complex viscous fluid-structure interactions. CFD methods have been applied, among others, in the following analyses of marine engineering applications: moored semi-submersibles in the ocean [9], slamming and green water loads on ships sailing in regular waves [10], added power prediction of ships sailing in head and oblique waves [11], and floating offshore wind turbines [12]. In addition, Koop [13] utilized CFD to determine the scale effects on current loads of offshore vessels in a side-by-side configuration. Further, Lu *et al.,* [14] reported results of a numerical study of fluid resonance in two narrow gaps of three identical rectangular structures. They identified an effect of the narrow gap, which results in wave-structure interactions in the band of resonant frequencies.

Zhao *et al.,* [15] give a comprehensive review on recent problems with side-by-side offloading floating liquefied natural gas (FLNG). The side-by-side offloading from the FLNG to the shuttle tanker is relatively new, for which limited guidelines are available. Thus, research regarding hydrodynamic interaction is needed for safe operation at sea. There are three factors affecting the operability of FLNG offloading, i.e., roll motions, tank sloshing, and the free surface motion in the vessel's gap. Further utilization of CFD in predicting the operability of FLNG is carried out for the evaluation of dynamic motion prediction of the coupled offloading system of FLNG [16] and hydrodynamic interactions of side-by-side FLNG-LNG carrier [17, 18]. In addition to current loads, the motion prediction is subjected to wave loads [19]. Previous studies emphasized the importance of validating the loads in the design phase of offshore structures. The loads can be obtained from laboratory model-scale experiments, full-scale measurements, or theoretical methods.

There are numerous attempts to benchmark the hydrodynamic interactions between two adjacent floating structures under wave loads. The benchmarking process involved developing a laboratory-scale experimental model in a towing tank and comparing the experimental results with numerical model results [20]. Some benchmark studies are as follows: a comparative study conducted numerically to analyze the effects of ship-to-ship and ship-to-wall interactions [21], ship-shaped floating structures in a side-by-side configuration [22], and two adjacent identical floating boxes modeled using a CFD approach in zero Froude number [23]. Intriguing observations concerning the hydrodynamic interactions of two floating structures are that the gap between them significantly affects the loads acting on them, and the gap also affects the wave amplitude inside the gap.

Studies utilizing CFD to investigate wave resonance phenomena in the context of two identical non-ship-like objects have also been reported in the literature. Jiang *et al.,* [24] conducted CFD simulations on two side-by-side boxes to investigate wave resonance phenomena. The simulation results revealed that the gap between the models greatly influenced the transmission of waves. Furthermore, the waves occurring within the gap significantly impacted the wave loads acting on the models. Similarly, He *et al.,* [25] and Jiang *et al.,* [26] also reported similar findings, emphasizing the

significant influence of the gap on wave transmission and the resulting wave forces affecting the motions of the boxes.

Following the recommendations of the International Towing Tank Conference (ITTC) [27], various research institutions and scholars conducted CFD benchmark studies on side-by-side floating structures in waves. Although many benchmark studies have been carried out, there is still a need to increase the accuracy of the results and to quantify the associated uncertainties. Considering the CFD method, there are uncertainties in the results of the six degrees of freedom motions, the wave height in the gap, and the forces acting on each body. These uncertainties stem from the model geometry, mass properties, and mooring setup. Considering experimental model tests, some uncertainties include the test model, instrumentation, initial test conditions, and human factors. In many cases, benchmark parameters are utilized in the benchmarking process to fit the experimental data. In addition to accuracy and uncertainties, the available scientific publications on benchmark CFD studies and their findings cannot easily be accessed, as indicated by Wei [28] and Peng *et al.,* [29]. Therefore, further benchmark study is necessary to consider the fluid flow computation, rigid body motion, and interactions between adjacent floating structures. The purpose of this study is to contribute to the ongoing process of CFD model benchmarking by examining the hydrodynamic interactions of two ship-like floating structures in waves, taking into account the viscous character of the fluids.

2. Methodology

A computational fluid dynamics (CFD) method is utilized in this study to investigate the hydrodynamic interactions of two ship-like structures in regular waves with varying gap between them. The gap is varied as d = (1/2)B, B and 2B, where d is the gap and B is the breadth of the floating structure. Further, we considered three ratios of wave length to vessel's length that are λ/L = 0.65, 1.5 and 2.0. λ stands for the wave length and L is the length of the floating structure (see Figure 1). The CFD method is described in more details in the following sub-sections.

2.1 Governing Equations

The unsteady Reynolds-Averaged Navier-Stokes (URANS) method was employed in this study to predict the motion responses of two adjacent ship-like structures under regular waves at zero-forward speed. The URANS method combines the Reynolds-averaging technique with unsteady flow assumptions to capture the time-averaged behavior of the fluid flow.

The URANS approach simulates the flow field and the motions of the floating structure by solving the Reynolds-averaged Navier-Stokes (RANS) equations and the equations for rigid-body motions of the floating structure. The RANS equations, which describe the flow field of unsteady, three-dimensional incompressible fluid, are given as follows:

$$\frac{\partial U_i}{\partial x_i} = 0 \tag{1}$$

$$\frac{\partial U_i}{\partial t} + \frac{\partial (U_i U_j)}{\partial x_j} = -\frac{1}{\rho}\frac{\partial P}{\partial x_i} + \frac{\partial}{\partial x_j}\left[\nu\left(\frac{\partial U_i}{\partial x_i} + \frac{\partial U_j}{\partial x_i}\right)\right] - \frac{\partial \overline{(u_i' u_j')}}{\partial x_j} + f_i \tag{2}$$

In Eq. (1) and Eq. (2), t is time, and i, j take values of 1, 2, or 3, U_i is the component of the time-averaged velocity, P is the time-averaged pressure, ρ is the fluid density, v is the kinematic viscosity

of the fluid, u_i' is the fluctuation of the velocity component, $-\rho\overline{u_i'u_j'}$ is the Reynolds stress tensor, and f_i represents the body force component resulting from gravitational acceleration.

For calculating the rigid body motions in the six degrees of freedom (6-DOF), it is necessary to determine the forces and moments acting on the rigid body mass [30]. The equations for the floating body motions are represented as follows:

$$(m + a_z)\ddot{z} + b\dot{z} + cz + d\ddot{\theta} + e\dot{\theta} + h\theta = F(t) \tag{3}$$

$$\left(I_{yy} + A_{yy}\right)\ddot{\theta} + B\dot{\theta} + C\theta + D\ddot{z} + E\dot{z} + Hz = M(t) \tag{4}$$

In Eq. (3) and Eq. (4), *m* is the rigid body mass, *a* is the rigid body added mass, *I* is an inertial mass moment, and $\ddot{z}, \dot{z}, z, \ddot{\theta}, \dot{\theta}, \theta$ denote the absolute motion variables of the floating body. Then, *F* is the excitation force, and *M* is the excitation moment. Eq. (3) represents the equation of motion that incorporates all the forces, while Eq. (4) represents the equation of angular motion that represents the moment of force.

This study's modeling design incorporates heave, pitch, and roll motions. To derive the 3 degrees of freedom (3-DOF) motion, the researchers calculate the velocity and pressure fields of the fluid domain. The linear and momentum equations capture the interaction between the fluid and the body [31] to achieve it. The following equations for this purpose:

$$\sum \vec{F} = m\vec{a} \tag{5}$$

$$\sum \overrightarrow{M_G} = I_G\overrightarrow{\alpha_G} + \vec{\omega} \times I_G\vec{\omega} \tag{6}$$

In Eq. (5) and Eq. (6), *F* represents the total force, *m* is the mass, and *a* is the acceleration. Meanwhile, *M* denotes the moment about the center of gravity of the rigid body, *I* represents the inertial mass moment, α is the angular acceleration, and ω is the angular speed.

Viscous shear stress acts parallel to the plane of the rigid body, while pressure acts perpendicular to it. Then, the motion of the floating structure is determined based on the velocity and pressure occurring in the flow field. The rigid body responds to the incident waves, causing changes in its position. These changes are then recalculated iteratively to determine the wave-induced forces.

2.2 Geometry of the Floating Structure Configurations, and Flow Similarities

The floating structure utilized in this study has a simple geometry, which consists of a box shape and two half cylinders. The box shape represents the parallel middle body of a ship, while the half cylinders represent the bow and stern. Two ship-like floating structures as described above were considered in the experiments with varying separation distance or gap between them. The gap, *d* is defined as distance between inner sides of the two vessels. The ITTC recommends these model configuration for a benchmark study of CFD modeling of floating structure responses in waves. Figure 1 shows three configurations of two ship-like floating structures considered in this study.

The CFD simulations simulate the motions of a model of the (full-scale) floating structure with a geometrical scale of 1:80. To validate the CFD simulation results, they are compared with experimental results performed in a towing tank. Table 1 summarizes the main particulars and scales for the length and displacement. Since gravity force is the dominant force affecting the motions of a

floating structure, the kinematic similarity prescribes that the Froude number Fr of the model must be equal the Froude number of the prototype. The Froude number Fr is defined as

$$F_r = \frac{U^2}{gL}. \tag{7}$$

where *U*, *g*, and *L* denote velocity, gravitational acceleration, and length, respectively. The kinematic similarity prescribes that Fr for the model is equal to Fr of the full scale structure as follows:

$$\frac{U_f^2}{gL_f} = \frac{U_m^2}{gL_m} \tag{8}$$

Table 1
Main dimensions of ship models

Parameter	Symbol	Full scale	Model A	Model B	Dimension	Scale factor
Length	*L*	120 m	1.5 m	1.5 m	L	α
Breadth	*B*	24 m	0.3 m	0.3 m	L	α
Depth	*D*	18 m	0.225 m	0.225 m	L	α
Draft	*T*	7.2	0.09 m	0.09 m	L	α
Displacement	Δ	6,912,000 kg	32 kg	32 kg	M	α^3
Gap	*d*	24 m	0.3 m	0.3 m	L	α
Wavelength	λ	240 m	3.0 m	3.0 m	L	α

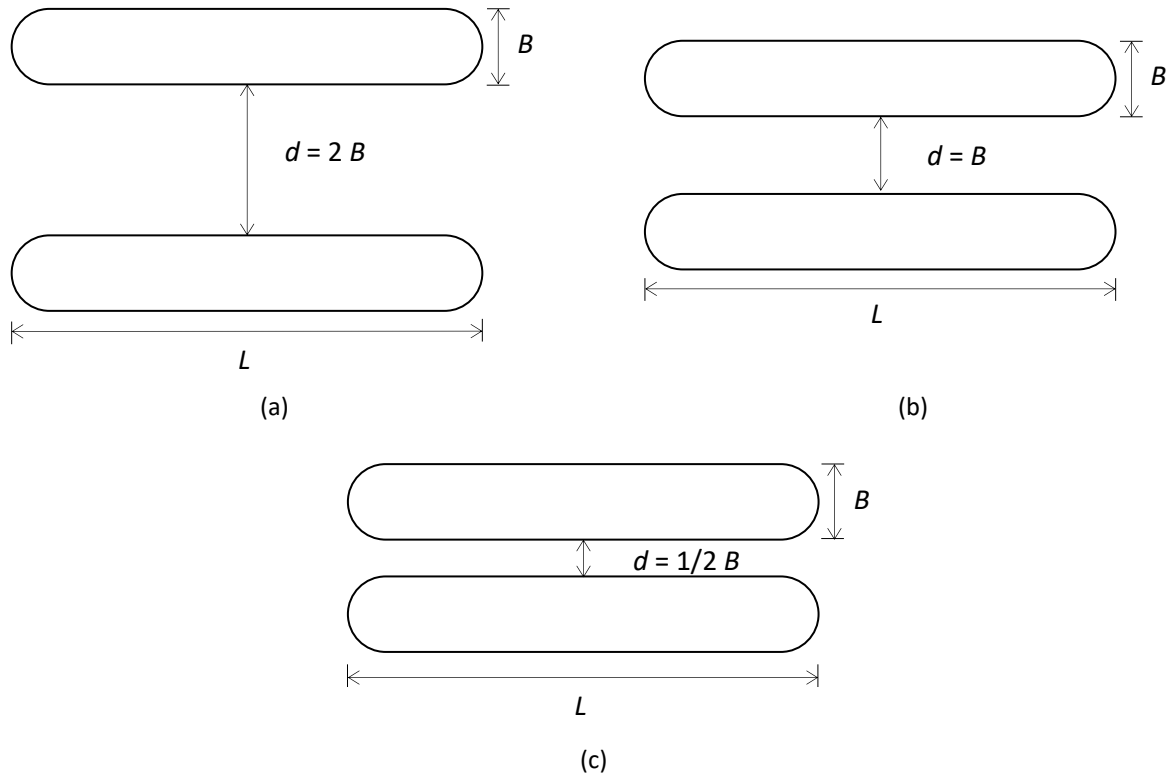

Fig. 1. Configuration of two ship-like structures considered in this study (a) *d* = 2*B*, (b) *d* = *B*, (c) *d* = (1/2) *B*

2.3 Computational Domain and Meshing

Figure 2 shows the computational domain used for the simulations with the floating structure located inside it. The computational domain is bounded by domain boundaries, defined as inlet, outlet, side wall, bottom wall, top opening and a symmetry plane. An overset grid-generation method was utilized for the meshing of the computational domain, where first a background domain is defined and latter an overset domain. The basic concept for meshing the background domain is similar to that for meshing the overset domains.

A structured grid was utilized employing 3-dimensional H-type hexahedral cells. The overset mesh particularly aimed at capturing the free surface and flow details near the hull of the floating structure. The other regions were meshed by using a coarser grid of the background mesh. This overset grid configuration allows for efficient mesh distribution and economic computational cost. This overset grid system was also utilized to calculate the 3-DOF rigid body motions along with the forces and moments contributing to vessel motions. This overset grid technique has been successfully implemented in previous studies of CFD simulations of floating vessel motions such as those reported by Jiao and Huang [32] and Chen and Hall [33]. Figure 3 shows the grid employed near the wall of the floating structure to capture the boundary-layer flow.

In summary, grid gradation was employed to simulate the rigid body motions by applying finer mesh near the wall and the free surface. The free surface is an interface between two different fluids, namely water and air. In addition, when generating regular waves with a prescribed wave height and wavelength, a minimum of ten cells was required to capture the wave height and one hundred cells to capture the wavelength. So, the grid gradation is finer near the hull and the free surface than that far from the hull and the free surface. Capturing the turbulent structures near the hull is critical for accurate calculations of the hydrodynamic loads and motion responses.

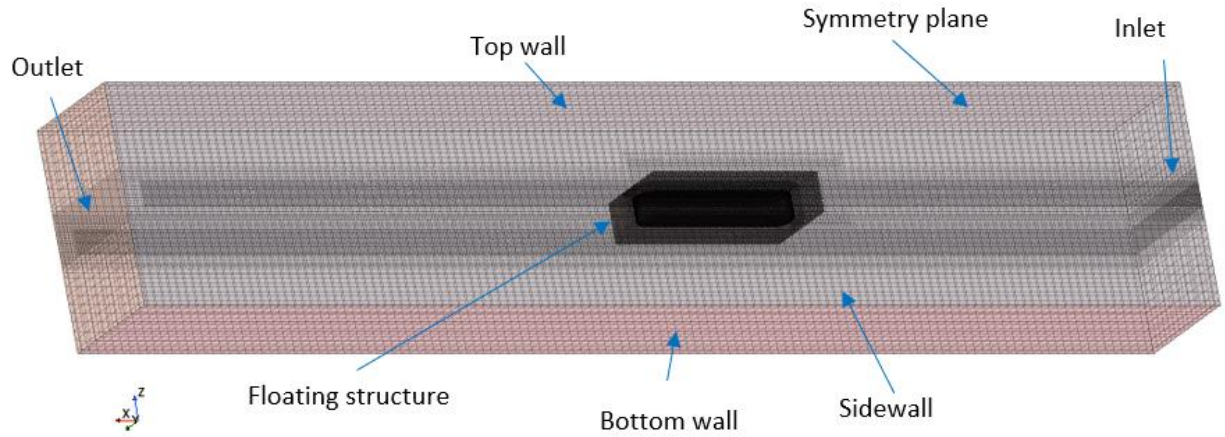

Fig. 2. Computational domain with the floating structure located in it and bounded by inlet, outlet, side wall, bottom wall, top wall and a symmetry plane

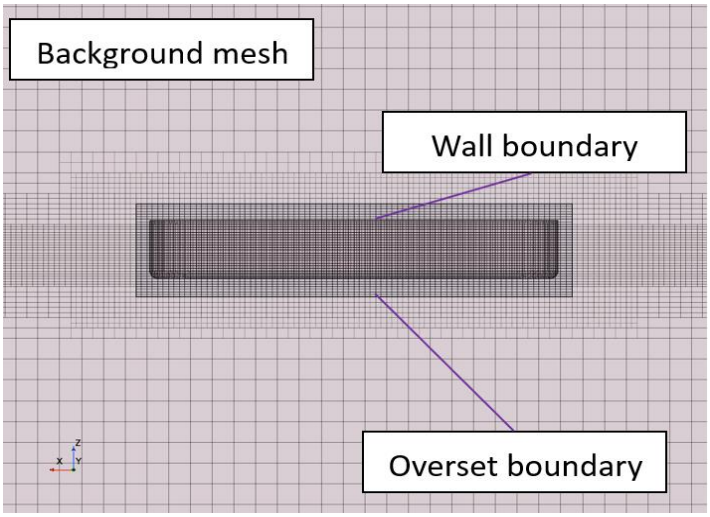

Fig. 3. Grid gradation showing finer mesh near the hull and the free surface

2.4 Boundary Conditions and Turbulence Model

The boundary conditions are defined as follows (see Figure 2). The hull of the floating structures is treated as wall with a no-slip condition, in the inlet a velocity inlet is defined, at the outlet a pressure outlet is defined, at the side wall, bottom wall and symmetry plane, symmery boundary conditions are applied, and at the top opening the air can flow freely from the atmosphere. Waves were generated at the inlet where Stokes 5th-order waves were utilized. The waves propagated from the inlet to the outlet, where wave damping was placed at the outlet. Details of the boundary conditions in the context of modeling floating structure responses in waves can be found in Tezdogan *et al.,* [34].

The free-surface boundary condition, applied at the interface between the water and air, needs special attention. In order to distinguish the water and air-fluid phases, an Eulerian multiphase segregated flow model is employed with distinct conservation equations for each phase. In addition, the volume of fluid (VOF) model was utilized to capture the free surface [37]. The interface-capturing method is capable of solving complex flow problems such as modeling of breaking waves. In the VOF method, the transport equation for the volume fraction or phase fraction *c* is represented in integral form as follows:

$$\frac{\mathrm{d}}{\mathrm{d}t}\int_V c\,\mathrm{dV} + \int_S c(\mathbf{v}-\mathbf{v_b})\cdot\mathbf{n}\,\mathrm{dS} = 0 \tag{9}$$

The value of c is in the range $0 \le c \le 1$, where $c = 1$ represents water and $c = 0$ represents air.

The k-ε turbulence model was utilized to calculate the Reynolds stress tensor $-\rho\overline{u_i' u_j'}$ (see Eq. (2)). This turbulence model is a two-equation model that solves transport equations for the turbulence kinetic energy (k) and turbulence dissipation rate (ε), and subsequently to determine the eddy viscosity of turbulent flow. In the present case, turbulent flow modeling is important near the vessel hull, where large velocity gradient occurs. The hull surface is assumed to be smooth and impermeable. The k-ε turbulence model has long been employed, particularly in industrial applications. For instance, it has been used by Jiang *et al.,* [35] to solve the coupled equations of mooring lines and floating structures, and by Lu *et al.,* [36] to address the hydrodynamic interactions between ship and tug boat.

3. Mesh Quality Checks, Time-Step Setting, and Grid Independence Tests

The quality of the mesh for the simulations was checked in accordance to the recommendation given by Katz [38] and Park *et al.,* [39]. The criteria used for the mesh quality checks are skewness angle, face validity, cell quality metric, volume change metric, and chevron quality indicator. The results of the checks are summarized in Table 2, showing that the mesh satisfies all the prescribed criteria.

Table 2
Mesh quality checks for 2.5 million cells

Parameter	Results	Acceptable value	Remarks
Cell skewness angle	0 cells > 85 degree	< 85 degree	Accepted
Face validity	2.5M cells = 1	~ 1	Accepted
Cell quality metric	2.5M cells = 1	~ 1	Accepted
Volume change metric	2.5M cells = 0.3	> 0.01	Accepted
Chevron quality indicator	2.5M cells > 0.01	~ 0	Accepted

The simulation time step determines the convergence of the numerical calculations. The value of the time step was determined such that the Courant-Friedrichs-Lewy (CFL) number is less than one in all computational cells. In particular, for VOF applications, it is recommended that the CFL < 0.5 ~ 0.75 [40–42]. Further, to simulate rigid body motion under regular waves, the ITTC recommends using at least one hundred time steps per wave period. The CFL is defined as follows:

$$CFL = \frac{\Delta t \times u}{\Delta z} \tag{10}$$

where Δt is the time step, Δz is the vertical size of the wave refinement zone, and u denotes the wave speed. The time step chosen in this study Δt = 0.001 s, resulting in CFL < 0.75. This value of time step also satisfies the ITTC criterion for regular waves with height H = 5 cm and period T = 1.39 s (wave length λ = 3.0 m).

In addition to mesh quality checks and proper setting of the time step, grid independence tests were carried out to determine the most economic grid for the simulations. Figure 4 summarizes the grid independence tests conducted in this study. Three mesh resolutions were considered, namely, the ones with 1.8 million, 2.2 million and 2.5 million cells. As shown in Figure 4, no substantial differences in wave elevation were observed amongst the three mesh resolutions. To achieve more accurate results, the number of cells used in simulations was 2.5 million.

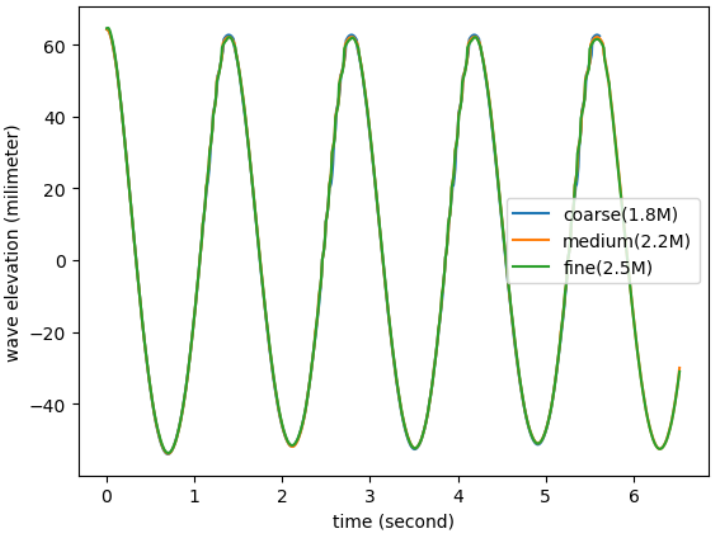

Fig. 4. Grid independence test results for wave elevation measured at the location of the floating structure

4. Validation of CFD Simulation Results

A validation of CFD codes refers to a check of the correctness of the physical models implemented in the numerical calculations. Usually, this is done by comparing the CFD results with experimental results. Further, a floating structure in waves has in general six-degree of freedom (6-DOF) motions, which are surge, sway, and heave for the translations, and roll, pitch, and yaw for the rotations. For a floating structure in head seas as considered in this study, the pitch motion is the most significant motion. Therefore, for the validation process, the pitch motion obtained from the CFD calculations will be compared with that obtained from a laboratory experiment.

Figure 5 shows a visualization of the vessel motion on the water surface obtained from a CFD simulation due to regular waves with wave height of 0.12 m and wave lenght of 3 m. In this visualization, the ratio of the wavelength to model length λ/L = 2.0. Figure 5 shows side view of snap shots at the instants t = 4.9, 5.2, 5.7 and 5.9 s. It can be seen in Figure 5 that the vessel undergoes a rather stationary periodic motion. The pitch motion of the vessel is clearly observed in Figure 5.

To see the pitch motion in more details, Figure 6 shows a comparison of the pitch motion time histories obtained from the CFD simulation and laboratory experiment for λ/L = 2.0 and gap $d = B$, where B is the width of the floating structure. Figure 6 shows that the phase of the motion obtained from the CFD is in a good agreement with that obtained from the experiment. However, there are some discrepancies in the magnitude (amplitude) of the motion, where the CFD results tend to underestimate the experimental data. The observed discrepancies may be ascribed to uncertainties in the CFD method and the experiment. In general, uncertainty in the geometrical model may be neglected, but uncertainty in mass distribution may result in such discrepancies. Similar results were reported earlier by Ardhiansyah *et al.,* [43]. Although further examination is necessary to account for uncertainties in the experiment, e.g., by analyzing the reflections of waves from the tank's end and investigating the tank side wall effects, Figure 6 shows that overall the CFD results are in a good agreement with the experimental results.

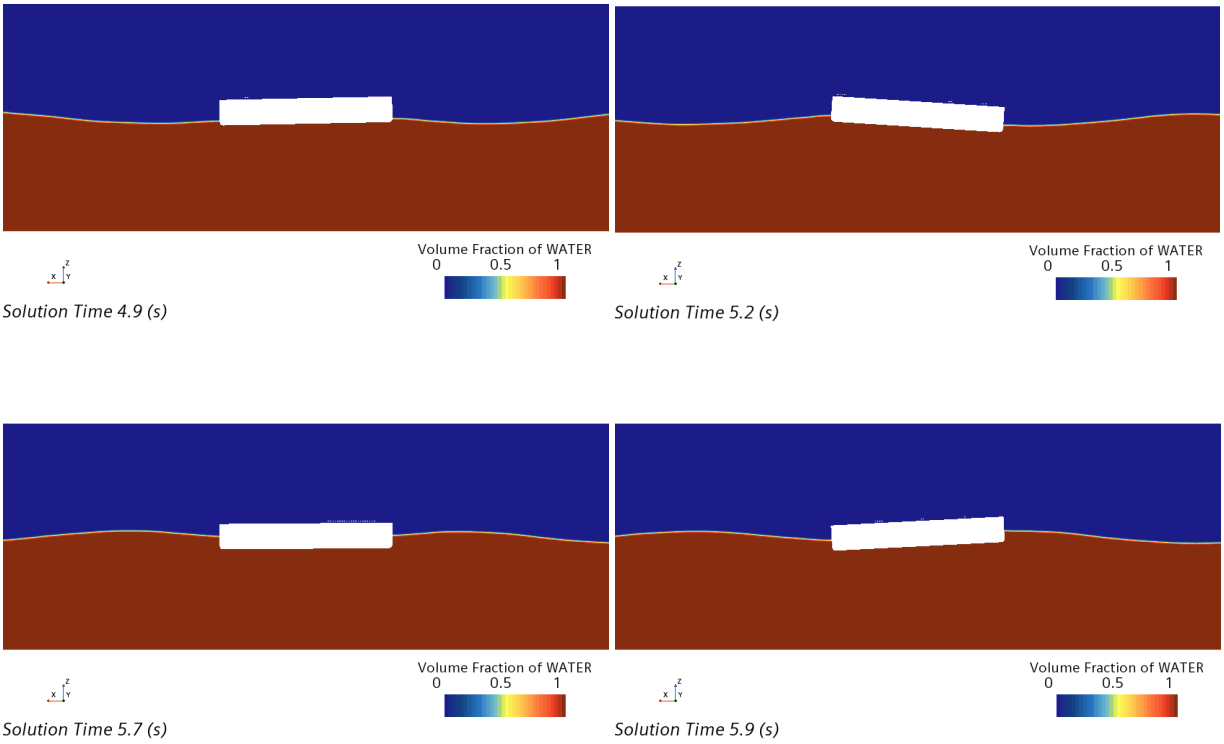

Fig. 5. Wave elevation and model motion at λ/L = 2.0

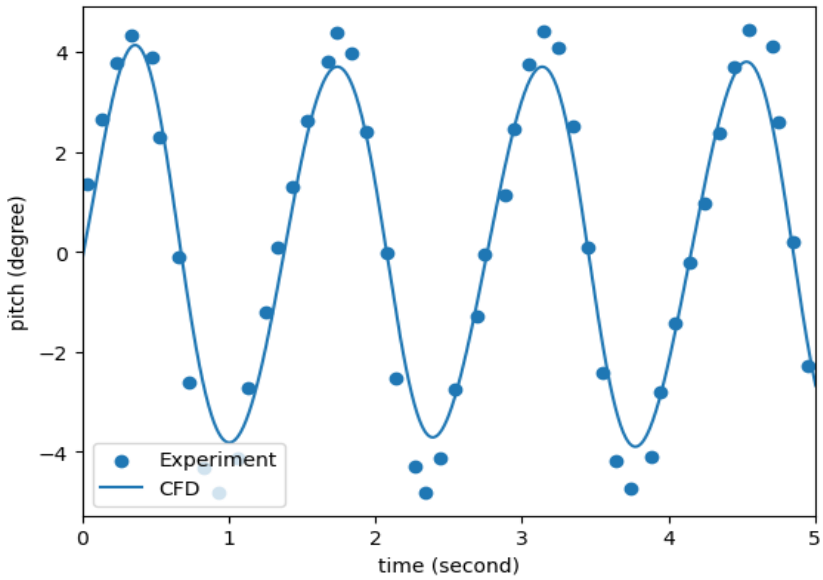

Fig. 6. Comparison of the pitch motion obtained from CFD simulation and laboratory experiment

5. Results and Discussion

5.1 Influence of Gap on the Wave Pattern

Figure 7 shows the wave patterns surrounding the floating vessels and the hull pressure experienced by the floating structures for λ/L = 2.0 and varying gap, namely, d = (1/2)B, B, and 2B. In Figure 7(a) diffracted waves are observed around the bow and stern of the vessels. The gap particularly affects the wave pattern inside the gap, where the gap determines the diffracted wave pattern inside the gap. At the smallest gap (d = (1/2)B) short crested waves are observed inside the gap, while at the gap d = B the wave crests in the gap show a rather straight pattern. Changes in the gap influence the wave elevation and the wave height inside the gap. The wave pattern outside the gap looks similar for all the three gaps. The pressure distribution on the side wall of the vessels in the gap is similar for all the three gaps considered as shown in Figure 7(b).

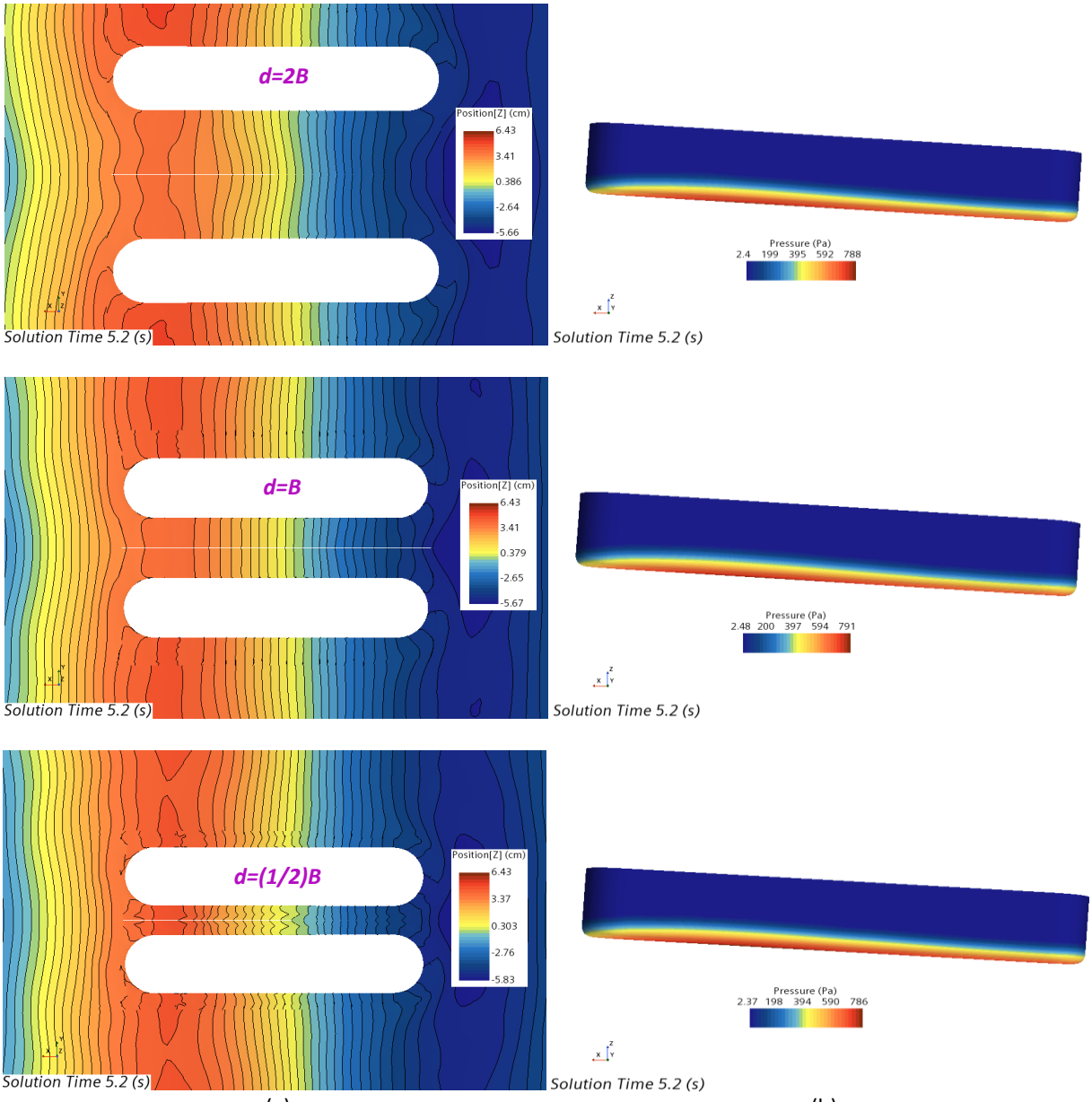

(a) (b)

Fig. 7. Wave pattern (a) and hull pressure distribution (b) for λ/L = 2.0 and varying gap (wave direction from right to left)

5.2 Influence of Wave Length on the Wave Pattern

Figure 8 shows the wave patterns for the gap d = (1/2)B and ratios of wave length to vessel's length λ/L = 0.65 and 1.5. The gap considered in this subsection is a rather narrow gap, for which in combination with rather high-frequency waves may result in wave resonance [23-25]. Figure 8 shows that the wave pattern for λ/L = 0.65 is very different from that for λ/L = 1.5. These wave patterns are in turn very different from that for λ/L = 2.0 described in Subsection 5.1. So, the wave length to the vessel's length ratio λ/L affects significantly the wave pattern around the vessels and inside the gap. The observed wave patterns in turn affect the motions of the vessels.

Further, an animation of the simulation results shows that the trapped waves are more easily released from the gap for λ/L = 0.65 than for λ/L = 1.5. The animation shows that the wave contours for λ/L = 0.65 propagate more easily through the gap between the floating vessels compared to the case with λ/L = 1.5.

The above findings align with the results reported by Meng [28], who conducted two-body hydrodynamic interaction experiments in waves, where the wave length to vessel's length ratio was chosen as λ/L = 0.65. He reported that nonlinear characteristics are noticeable particularly in high-frequency waves or short waves. The relationship between gap and wave height characteristics becomes nonlinear when the waves are shorter than the vessel length.

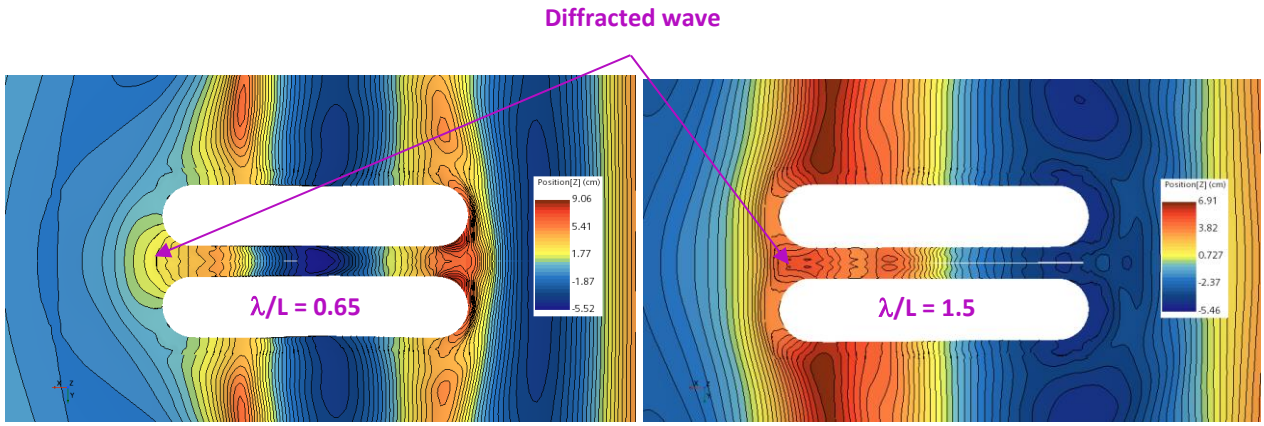

Fig. 8. Wave pattern for λ/L = 0.65 (left) and 1.5 (right) and gap d = *(1/2)B* (wave direction from right to left)

5.3 Influence of Gap on Hull Pressure Distribution

Figure 9 shows the hull pressure distribution on the vessel's keel for λ/L = 2.0 and varying gap, namely, d = (1/2)B, d = B, and d = 2B. The pressure distributions were taken at the instant t = 5.2 s, when the wave crest was at the stern of the vessels. For all three gaps variations, pressure distribution on each vessel are symmetry about the longitudinal axis between two vessels. Figure 9 shows that the three different gaps resulted in different pressure contours. However, despite the differences, they all have non-symmetric pressure contours about the center plane of the each vessel. The non-symmetric hull pressure distribution will result in roll motion eventhough the structure under pure head seas condition. This is because the non-symmetric pressure distribution will result in non-symmetric wave force acting on the floating structure. This observation is consistent with that reported by Gao *et al.,* [44] who found that the wave force distribution and flow patterns influence the vessel motion responses of the side-by-side floating structure. The side-by-side floating structures mutually influence each other's motion, resulting in motions that would not occur under a single-body condition.

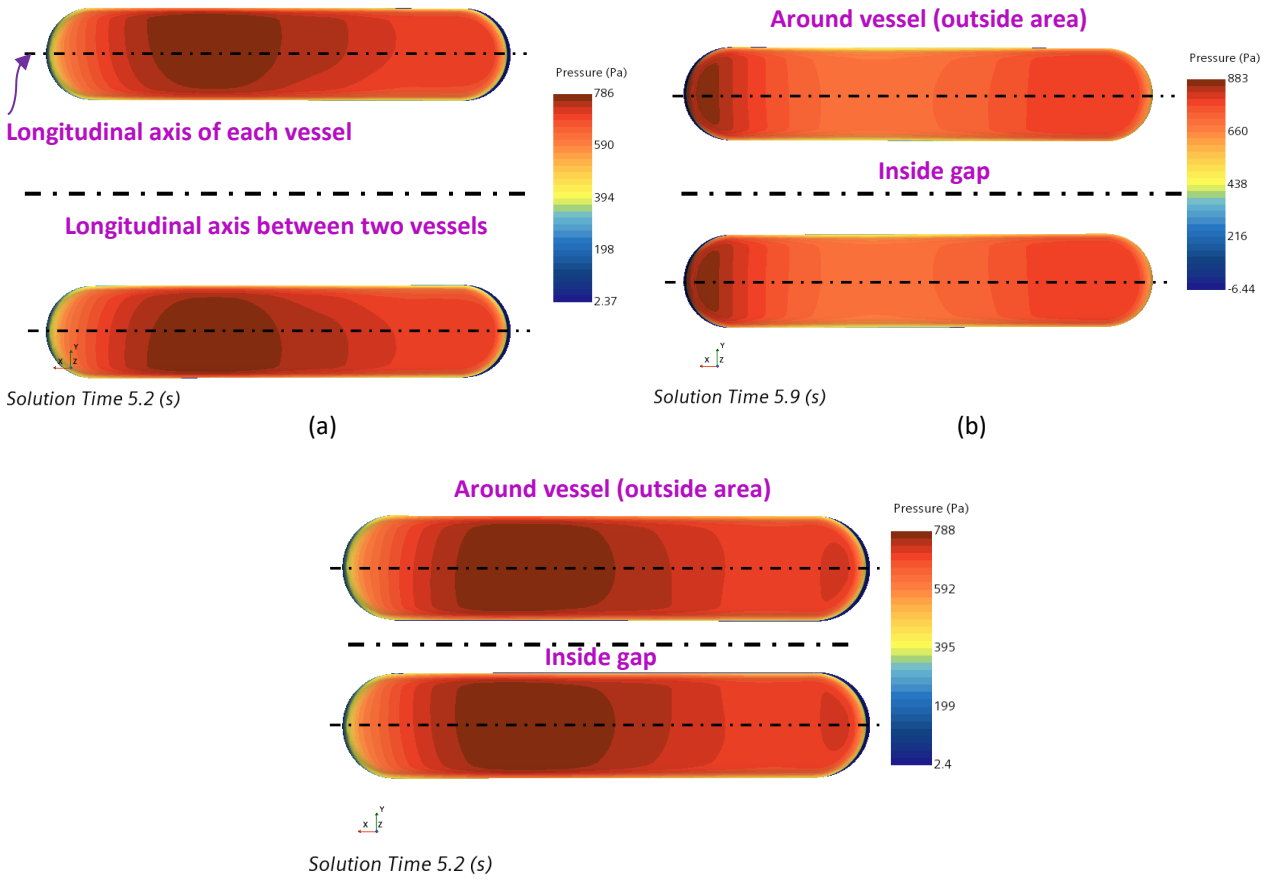

Fig. 9. Hull Pressure distribution for different gaps: (a) $d = 2B$, (b) $d = B$, and (c) $d = (1/2)\ B$

5.4 Influence of Gap on Vessel Motions

The heave, pitch and roll motions are examined for the case of relatively long waves at $\lambda/L = 2.0$ and varying gap, namely, $d = (1/2)B$, B and $2B$, where B is the width of the floating structure. Figures 10a, 10b and 11 show, respectively, the heave, pitch and roll motion time histories of the floating structure. Figure 10 shows that the heave and pitch motions display a rather regular pattern, although an amplitude modulation was observed. In contrast, Figure 11 shows that the roll motion exhibits a rather irregular pattern and the generation of side-band frequency components. Fourier analysis revealed that the fundamental component of the roll motion for all gaps has a period $T = 0.77$ s. The observed amplitude modulation and the generation of side-band frequency components indicate a non-linear interaction process. The non-linear process may arise due to coupled motions involving the interaction between the two floating structures, and being influenced by other modes of motions.

Figure 10 shows that the gap does not affect the frequency of the heave and pitch motions. Further, it affects the amplitude of the heave motion more significantly than that of the pitch motion. Figure 10(b) and 11 show that the gap has very little influence on the frequency and amplitude of the pitch motion, but it influences significantly the roll motion.

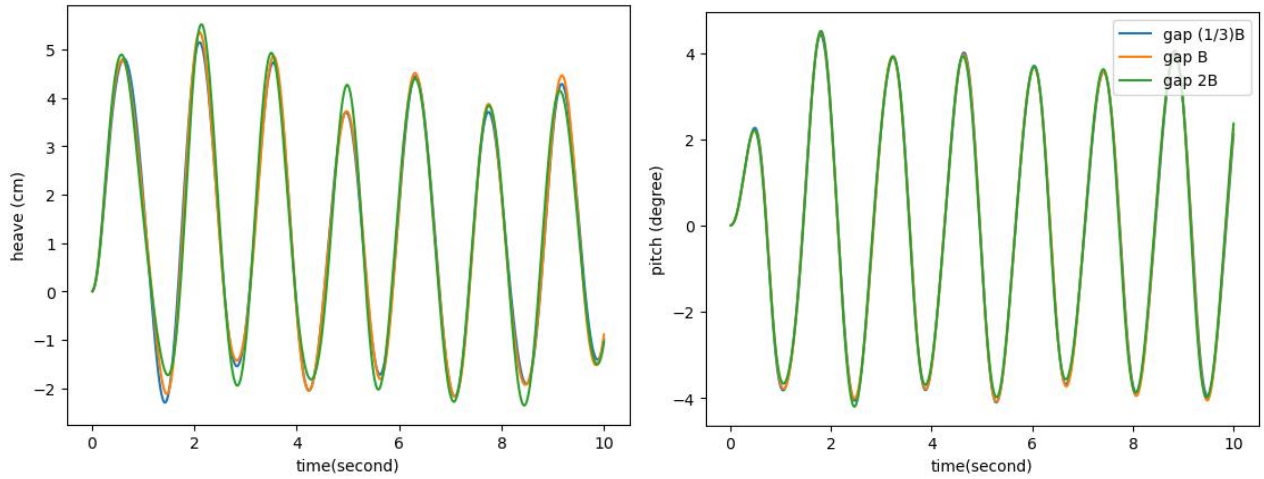

(a) (b)

Fig. 10. Heave (a) and pitch (b) motions for λ/L = 2.0 and different gaps, namely, d = (1/2)B, B and 2B

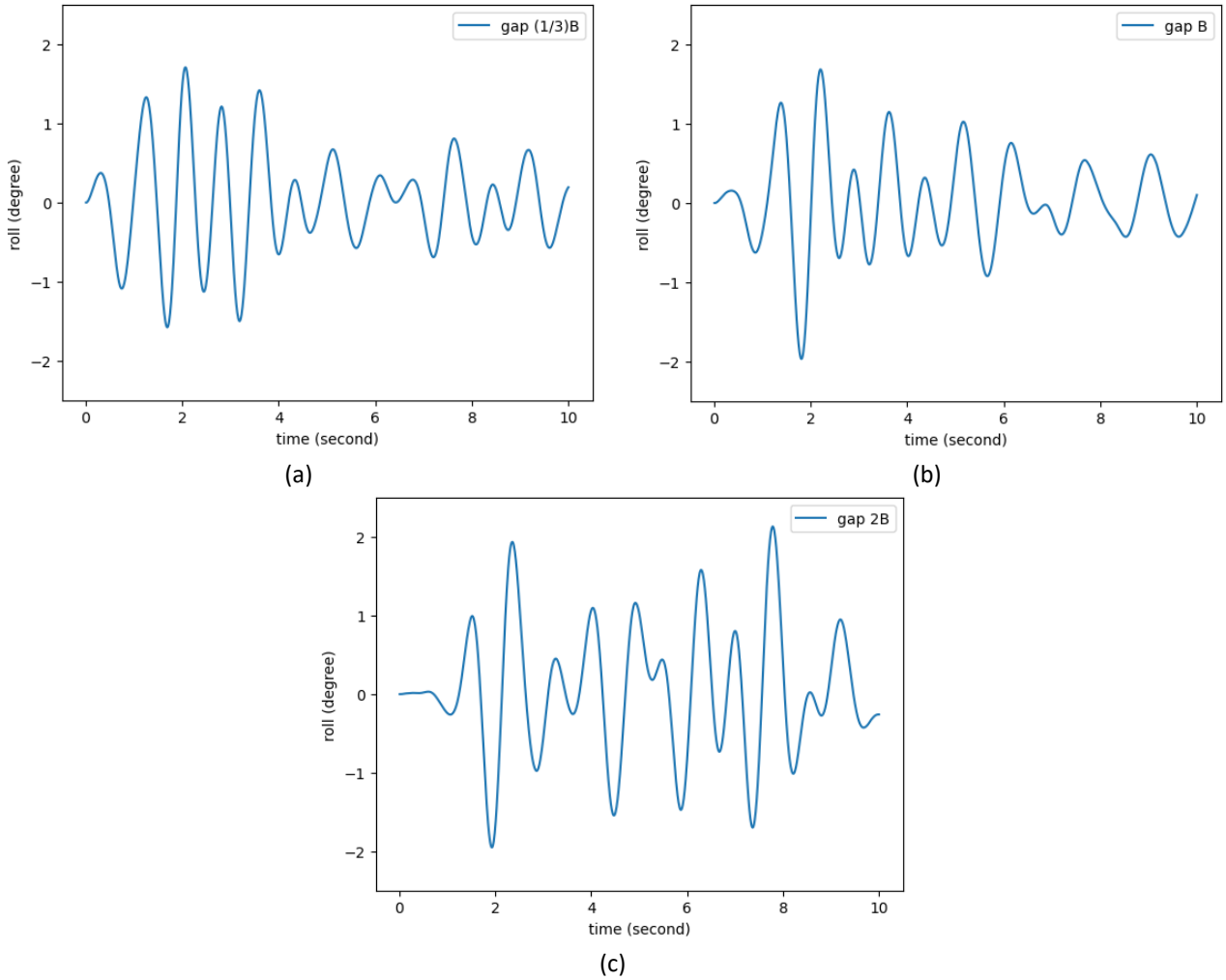

(a) (b)

(c)

Fig. 11. Roll motion for λ/L = 2.0 and different gaps (a) d = (1/2)B, (b) d = B, and (c) d = 2B

Figure 11 shows that roll motion occurs in all gap variations, with a maximum value approximately 2 degrees. Further, the gap d = 2B resulted in the largest roll motion. As observed in Subsection 5.3, the non-symmeric viscous force resulted in roll motion of the side-by-side vessels in head seas. The largest roll motion, which is observed for the gap d = 2B, is ascribed to the largest

viscous force acting on the floating structure. Further, a larger roll motion resulted in larger waves generated by the floating structure. This finding is consistent with that reported by Ok *et al.*, [45] who conducted a similar study on the interaction of two identical floating production, storage and offloading (FPSO) models in regular waves. Utilizing a potential theory would not reveal the obove observations. The CFD viscous fluid method overcomes the limitations of an ideal fluid method, as also emphasized by Pena and McDougall [46].

6. Conclusions

URANS CFD method was applied to study the hydrodynamic interactions of a side-by-side configuration of two ship-like structures in regular waves. Three ratios of wave length to vessel's length were considered, namely, λ/L = 0.65, 1.5 and 2.0. In addition, three gaps between the vessels were investigated, namely, d = (1/2)B, B and 2B, where B is the breadth of the vessel. Simulation results show that the wave length to vessel's length ratio λ/L affects significantly the wave pattern around the vessels and inside the gap. Diffracted waves were observed around the bow and stern of the vessels. For λ/L = 2.0 (longer waves) the gap affects particularly the wave pattern inside the gap. Outside the gap, the wave patterns look similar for all the three gaps. In contrast, for the shorter waves (λ/L = 0.65 and 1.5), the gap influences the wave pattern both inside and outside the gap. The trapped waves are more easily released from the gap for λ/L = 0.65 than for λ/L = 1.5. The observed wave patterns in turn affect the motions of the vessels.

Further, the pressure distribution on the keel surface of the vessels is asymmetric about the vertical center plane along the vessel. The observed pressure asymmetry results in asymmetric viscous forces, which ultimately resulted in roll motion eventhough the vessel is in head seas. The gap has very little influence on the frequency and amplitude of the pitch motion, but it influences significantly the roll motion. Amplitude modulation was observed in the heave and pitch motions, while generation of side-band frequency components were observed in the roll motion. The observed amplitude modulation and the generation of side-band frequency components indicate a non-linear fluid-structure interaction.

Acknowledgment

The authors gratefully acknowledge financial support from the Indonesian Ministry of Research and Higher Education and Institut Teknologi Sepuluh Nopember (Doctoral Dissertation Research scheme), Grant No. 084/E5/PG.02.00.PT/2022.

References

[1] Lewandowski, Edward M. "Multi-vessel seakeeping computations with linear potential theory." *Ocean engineering* 35, no. 11-12 (2008): 1121-1131. https://doi.org/10.1016/j.oceaneng.2008.04.011

[2] Yoo, Jung-Hee, Patrick Schrijvers, Arjen Koop, and Jong-Chun Park. "CFD Prediction of Wind Loads on FPSO and Shuttle Tankers during Side-by-Side Offloading." *Journal of Marine Science and Engineering* 10, no. 5 (2022): 654. https://doi.org/10.3390/jmse10050654

[3] Ha, Y. J., B. W. Nam, S. Y. Hong, D. W. Jung, and H. J. Kim. "Experimental and numerical study on mating operation of a topside module by a floating crane vessel in waves." *Ocean Engineering* 154 (2018): 375-388. https://doi.org/10.1016/j.oceaneng.2018.01.074

[4] Jiang, Zhiyu, Lin Li, Zhen Gao, Karl Henning Halse, and Peter Christian Sandvik. "Dynamic response analysis of a catamaran installation vessel during the positioning of a wind turbine assembly onto a spar foundation." *Marine Structures* 61 (2018): 1-24. https://doi.org/10.1016/j.marstruc.2018.04.010

[5] Aborgela, Taha, Ahmed S. Shehata, M. A. Kotb, and A. Radwan. "Heavy lift semi-submersible ships utilization in offshore wind turbines industry." *Energy Reports* 8 (2022): 834-847. https://doi.org/10.1016/j.egyr.2022.07.097

[6] Newton, R. N. "Some notes on interaction effects between ships close aboard in deep water." In *Proceedings of*

first symposium on ship maneuverability, DTMB Report, vol. 1461, pp. 1-24. 1960.
[7] Remery, G. F. "Mooring forces induced by passing ships." In *Offshore technology conference*, pp. OTC-2066. OTC, 1974. https://doi.org/10.4043/2066-MS
[8] Newman, J. N. "Application of generalized modes for the simulation of free surface patches in multi body hydrodynamics." *WAMIT Consortium report* (2003).
[9] Wang, Lu, Amy Robertson, Jang Kim, Hyunchul Jang, Zhi-Rong Shen, Arjen Koop, Tim Bunnik, and Kai Yu. "Validation of CFD simulations of the moored DeepCwind offshore wind semisubmersible in irregular waves." *Ocean Engineering* 260 (2022): 112028. https://doi.org/10.1016/j.oceaneng.2022.112028
[10] Jiao, Jialong, Songxing Huang, Tahsin Tezdogan, Momchil Terziev, and C. Guedes Soares. "Slamming and green water loads on a ship sailing in regular waves predicted by a coupled CFD–FEA approach." *Ocean Engineering* 241 (2021): 110107. https://doi.org/10.1016/j.oceaneng.2021.110107
[11] Sanada, Yugo, Dong-Hwan Kim, Hamid Sadat-Hosseini, Frederick Stern, Md Alfaz Hossain, Ping-Chen Wu, Yasuyuki Toda et al. "Assessment of EFD and CFD capability for KRISO Container Ship added power in head and oblique waves." *Ocean engineering* 243 (2022): 110224. https://doi.org/10.1016/j.oceaneng.2021.110224
[12] Clément, Constance, Pauline Bozonnet, Guillaume Vinay, Philippe Pagnier, Adria Borras Nadal, and Julien Réveillon. "Evaluation of Morison approach with CFD modelling on a surface-piercing cylinder towards the investigation of FOWT Hydrodynamics." *Ocean Engineering* 251 (2022): 111042. https://doi.org/10.1016/j.oceaneng.2022.111042
[13] Koop, Arjen. "Using CFD to determine scale effects on current loads of offshore vessels in side-by-side configuration." *Ocean Engineering* 195 (2020): 106707. https://doi.org/10.1016/j.oceaneng.2019.106707
[14] Lu, Lin, Liang Cheng, Bin Teng, and Ming Zhao. "Numerical investigation of fluid resonance in two narrow gaps of three identical rectangular structures." *Applied Ocean Research* 32, no. 2 (2010): 177-190. https://doi.org/10.1016/j.apor.2009.10.003
[15] Zhao, Wenhua, Ian Angus Milne, Michalakis Efthymiou, Hugh Alwyn Wolgamot, Scott Draper, P. H. Taylor, and R. Eatock Taylor. "Current practice and research directions in hydrodynamics for FLNG-side-by-side offloading." *Ocean Engineering* 158 (2018): 99-110. https://doi.org/10.1016/j.oceaneng.2018.03.076
[16] Zhao, Dongya, Zhiqiang Hu, Ke Zhou, Gang Chen, Xiaobo Chen, and Xingya Feng. "Coupled analysis of integrated dynamic responses of side-by-side offloading FLNG system." *Ocean Engineering* 168 (2018): 60-82. https://doi.org/10.1016/j.oceaneng.2018.08.016
[17] Jin, Yuting, Shuhong Chai, Jonathan Duffy, Christopher Chin, and Neil Bose. "URANS predictions on the hydrodynamic interaction of a conceptual FLNG-LNG offloading system in regular waves." *Ocean Engineering* 153 (2018): 363-386. https://doi.org/10.1016/j.oceaneng.2018.01.102
[18] Jin, Yuting, Shuhong Chai, Jonathan Duffy, Christopher Chin, Neil Bose, and Cameron Templeton. "RANS prediction of FLNG-LNG hydrodynamic interactions in steady current." *Applied Ocean Research* 60 (2016): 141-154. https://doi.org/10.1016/j.apor.2016.09.007
[19] Hirdaris, S. E., W. Bai, Daniele Dessi, Ayşen Ergin, X. Gu, O. A. Hermundstad, R. Huijsmans et al. "Loads for use in the design of ships and offshore structures." *Ocean engineering* 78 (2014): 131-174. https://doi.org/10.1016/j.oceaneng.2013.09.012
[20] Qiu, Wei, Wei Meng, Heather Peng, Jiacheng Li, Jean-Marc Rousset, and Claudio A. Rodríguez. "Benchmark data and comprehensive uncertainty analysis of two-body interaction model tests in a towing tank." *Ocean Engineering* 171 (2019): 663-676. https://doi.org/10.1016/j.oceaneng.2018.11.057
[21] Degrieck, Augustijn, Bryan Uyttersprot, Serge Sutulo, Carlos Guedes Soares, Wim Van Hoydonck, Marc Vantorre, and Evert Lataire. "Hydrodynamic ship–ship and ship–bank interaction: A comparative numerical study." *Ocean Engineering* 230 (2021): 108970. https://doi.org/10.1016/j.oceaneng.2021.108970
[22] Xu, Xiaosen, Prasanta Sahoo, Johanna Evans, and Yanwu Tao. "Hydrodynamic performances of FPSO and shuttle tanker during side-by-side offloading operation." *Ships and Offshore Structures* 14, no. sup1 (2019): 292-299. https://doi.org/10.1080/17445302.2019.1580845
[23] Gao, Junliang, Shukai Gong, Zhiwei He, Huabin Shi, Jun Zang, Tao Zou, and Xu Bai. "Study on wave loads during steady-state gap resonance with free heave motion of floating structure." *Journal of Marine Science and Engineering* 11, no. 2 (2023): 448. https://doi.org/10.3390/jmse11020448
[24] Jiang, Sheng-Chao, Wei Bai, and Bin Yan. "Higher-order harmonic induced wave resonance for two side-by-side boxes in close proximity." *Physics of Fluids* 33, no. 10 (2021). https://doi.org/10.1063/5.0065407
[25] He, Zhi-wei, Jun-liang Gao, Hua-bin Shi, Jun Zang, Hong-zhou Chen, and Qian Liu. "Investigation on effects of vertical degree of freedom on gap resonance between two side-by-side boxes under wave actions." *China Ocean Engineering* 36, no. 3 (2022): 403-412. https://doi.org/10.1007/s13344-022-0036-5
[26] Jiang, Sheng-Chao, Hao Liu, Tie-Zhi Sun, and Qian Gu. "Numerical simulation for hydrodynamic behavior of box-systems with and without narrow gaps." *Ocean Engineering* 214 (2020): 107698. https://doi.org/10.1016/j.oceaneng.2020.107698

[27] ITTC, "The Ocean Engineering Committee Final Report and Recommendations to the 25th ITTC," I, pp. 263–324, (2021).
[28] Meng, Wei. "Numerical and experimental studies of two-body hydrodynamic interaction in waves." PhD diss., Memorial University of Newfoundland, 2020.
[29] Peng, Heather, Md Ashim Ali, and Wei Qiu. "Hydrodynamic interaction of two bodies in waves." In *30th International Workshop on Water Waves and Floating Bodies, Bristol, UK*. 2015.
[30] Bhattacharyya, Rameswar. "Dynamics of marine vehicles." *(No Title)* (1978).
[31] Cakici, Ferdi, Omer Faruk Sukas, Omer Kemal Kinaci, and Ahmet Dursun Alkan. "Prediction of the vertical motions of dtmb 5415 ship using different numerical approaches." *Brodogradnja: Teorija i praksa brodogradnje i pomorske tehnike* 68, no. 2 (2017): 29-44. https://doi.org/10.21278/brod68203
[32] Jiao, Jialong, and Songxing Huang. "CFD simulation of ship seakeeping performance and slamming loads in bi-directional cross wave." *Journal of Marine Science and Engineering* 8, no. 5 (2020): 312. https://doi.org/10.3390/jmse8050312
[33] Chen, Haifei, and Matthew Hall. "CFD simulation of floating body motion with mooring dynamics: Coupling MoorDyn with OpenFOAM." *Applied Ocean Research* 124 (2022): 103210. https://doi.org/10.1016/j.apor.2022.103210
[34] Tezdogan, Tahsin, Atilla Incecik, and Osman Turan. "Full-scale unsteady RANS simulations of vertical ship motions in shallow water." *Ocean Engineering* 123 (2016): 131-145. https://doi.org/10.1016/j.oceaneng.2016.06.047
[35] Jiang, Changqing, Ould el Moctar, Guilherme Moura Paredes, and Thomas E. Schellin. "Validation of a dynamic mooring model coupled with a RANS solver." *Marine Structures* 72 (2020): 102783. https://doi.org/10.1016/j.marstruc.2020.102783
[36] Zou, Lu, Zao-jian Zou, and Yi Liu. "CFD-based predictions of hydrodynamic forces in ship-tug boat interactions." *Ships and Offshore Structures* 14, no. sup1 (2019): 300-310. https://doi.org/10.1080/17445302.2019.1589963
[37] Muzaferija, Samir. "Computation of free surface flows using interface-tracking and interface-capturing methods." *Nonlinear water-wave interaction. Computational Mechanics, Southampton* (1998).
[38] Katz, Aaron, and Venkateswaran Sankaran. "Mesh quality effects on the accuracy of CFD solutions on unstructured meshes." *Journal of Computational Physics* 230, no. 20 (2011): 7670-7686. https://doi.org/10.1016/j.jcp.2011.06.023
[39] Park, Gwanyong, Changmin Kim, Minhyung Lee, and Changho Choi. "Building geometry simplification for improving mesh quality of numerical analysis model." *Applied Sciences* 10, no. 16 (2020): 5425. https://doi.org/10.3390/app10165425
[40] ITTC, "Practical Guidelines for Ship CFD Applications," *ITTC – Recommended Procedures and Guidelines ITTC*, pp. 1–8, (2011).
[41] Silva, Daniel FC, Paulo TT Esperança, and Alvaro LGA Coutinho. "Green water loads on FPSOs exposed to beam and quartering seas, Part II: CFD simulations." *Ocean Engineering* 140 (2017): 434-452. https://doi.org/10.1016/j.oceaneng.2016.11.008
[42] Palm, Johannes, and Claes Eskilsson. "Mooring systems with submerged buoys: Influence of buoy geometry and modelling fidelity." *Applied Ocean Research* 102 (2020): 102302. https://doi.org/10.1016/j.apor.2020.102302
[43] Ardhiansyah, Fahmy, Eko Budi Djatmiko, and Rudi Walujo Prastianto, "Experimental Study of Wave Resonance and Motion Response in Side-by-Side Ships," in *International Conference and Exhibition on Sustainable Energy and Advanced Materials*, 2022.
[44] Gao, Qingze, Lifei Song, and Jianxi Yao. "Rans prediction of wave-induced ship motions, and steady wave forces and moments in regular waves." *Journal of Marine Science and Engineering* 9, no. 12 (2021): 1459. https://doi.org/10.3390/jmse9121459
[45] Ok, H. T., S. J. Lee, and J. H. Choi. "Numerical simulation of motion of single and side-by-side vessels in regular waves using OpenFOAM." *Ships and Offshore Structures* 12, no. 6 (2017): 793-803. https://doi.org/10.1080/17445302.2016.1265697
[46] Peña, Blanca, and Aaron McDougall. "An investigation into the limitations of the panel method and the gap effect for a fixed and a floating structure subject to waves." In *International Conference on Offshore Mechanics and Arctic Engineering*, vol. 49989, p. V007T06A048. American Society of Mechanical Engineers, 2016. https://doi.org/10.1115/OMAE2016-54121